

Article

Electrospun Porous PDLA Fiber Membrane Coated with nHA

Linhui Qiang ^{1,2,*} , Cong Zhang ³, Feng Qu ¹, Xiaonan Wu ¹ and Hongyan Wang ^{2,*}

¹ Department of Chemical Engineering, Chengde Petroleum College, Chengde 067000, China; cdpc_qf@sina.com (F.Q.); wuxn_cdpc@163.com (X.W.)

² College of Chemistry, Jilin University, Changchun 130012, China

³ United Microchip Corporation Integrated Circuit Manufacture (Xiamen) Co., Ltd., Xiamen 361000, China; zhangc_uscxm@sina.com

* Correspondence: qianglinhui@163.com (L.Q.); why_jlu@126.com (H.W.)

Received: 25 April 2018; Accepted: 18 May 2018; Published: 21 May 2018



Featured Application: The PDLA/nHA composite fibrous membrane has potential application value as scaffold material in tissue engineering.

Abstract: Porous poly- D, L-lactic acid (PDLA) electrospinning fiber membrane was prepared, and nano-hydroxyapatite (nHA) was adsorbed and wrapped into it during the unique shrinking process of the PDLA fiber membrane to fabricate the PDLA/nHA composite membrane scaffold for tissue engineering. Compare with the composite fibers prepared by blend electrospinning, most of nHA particles are observed to distribute on the surface of new type composite fibers, which could significantly improve the water wettability and induce the cellular adherence. FTIR analysis indicated that the PDLA/nHA composite fibrous membrane was formed by physical adsorption. The combination was probed by scanning electron microscope, thermo-gravimetric, water contact angle and mechanical property analysis. It was proved that the nHA particles' content and distribution, surface wettability, modulus and tensile strength of PDLA/nHA composite fibrous membrane were influenced by the concentration of nHA dispersion and pores on the PDLA fiber surface. The 10.6 wt % PDLA/nHA composite fibrous membrane exhibits a more balanced tensile strength (3.28 MPa) and surface wettability (with a water contact angle of 0°) of the composite mats. Scanning electron microscope and confocal laser scanning microscopy images of chondrocyte proliferation further showed that the composite scaffold is non-toxic. The adherence and proliferation of chondrocytes on the 10.6 wt % PDLA/nHA fibrous membrane was significantly improved, compared with PDLA mat. The 10.6 wt % PDLA/nHA composite fibrous membrane has potential application value as scaffold material in tissue engineering.

Keywords: poly-D-L-lactic acid; hydroxyapatite; composite fibrous membrane; electrospinning; tissue engineering

1. Introduction

Tissue defects arising from trauma, tumor or other diseases already lead to a large number of tissue-repair operations being performed worldwide every year, causing extensive physical and mental suffering for patients [1,2]. At present, the tissue graft for tissue repair is transplanted from another part of the recipient's body or by allografts. The shortage of tissue graft donors and the significant post-operative morbidity have been major problems in tissue grafting solutions [2,3]. Tissue engineering has provided a new approach for tissue repair. Once the autologous cells take hold and grow on the scaffold, the tissue engineering scaffold can be transplanted into the patient without fear

of rejection. Furthermore, the tissue repair is not limited by an insufficient supply of tissue donor tissue or by donor morbidity risks [4,5].

One of the core technologies intrinsic to tissue engineering is the construction of an engineering scaffold, which focuses on materials and structures of scaffolds for cell seeding and in vitro or in vivo culturing. The scaffolds should not only possess excellent biocompatibility [6,7], but also have a reasonable three-dimensional structure [8], surface wettability [9] and so on [10–12]. Therefore, tissue engineering scaffolds with excellent performance are interesting to many researchers [13–15]. In recent years, polylactide/hydroxyapatite (PLA/HA) composites specially prepared by electrospinning have been an excellent tissue engineering scaffold [16–19]. The PLA-based biopolymer fiber framework has a controllable 3-D network structure, good mechanical behavior, biocompatibility and biodegradability [20,21]. Hydrophilic HA acts to improve the water wettability, induce the cellular adherence and provide additional functionality [22–24]. Nevertheless, there are many HA particles distributed on the inside of PLA-based nanofiber, prepared by blend electrospinning, which could not effectively improve the water wettability and induce the cellular adherence. To overcome this issue and to increase the exposed area of the HAs to cells, new processing strategies are required.

In this paper, a novel method is presented for the preparation of poly-D-L-lactic acid (PDLLA) fibrous membrane embedded with nano-hydroxyapatite (nHA) particles for tissue engineering scaffold. Almost all the nHA particles are observed to distribute on the surface of new type composite fibers, which could significantly improve the water wettability and induce the cellular adherence. Two steps were involved in this method. First, a phase separation method was employed to prepare the porous PDLLA fibrous membrane. Second, the PDLLA/nHA composite fibrous membranes were fabricated by immersing the porous PDLLA into nHA dispersions, which were then shrunk in absolute ethanol. Composite fibrous mats were characterized for their surface topography, nHA content, surface wettability and mechanical behavior, amongst other features. Finally, cell proliferation experiments using rabbit chondrocytes were performed on the PDLLA/nHA composite membrane, bringing about potential applications in tissue engineering.

2. Materials and Methods

2.1. Materials

PDLLA ($M_w = 400,000$, from the Shandong Institute of Medical Appliances, Jinan, China) was used as the materials for electrospinning. Dichloromethane (DCM) purchased from Sigma-Aldrich Co. (St. Louis, MO, USA) was used as the solvent for electrospinning. Calcium hydroxide ($\text{Ca}(\text{OH})_2$) and phosphoric acid (H_3PO_4) were used for synthesizing the nHA particles. All other chemicals and reagents were purchased from Sinopharm Chemical Reagent Co., Ltd. (Beijing, China).

2.2. Synthesis

2.2.1. Preparation of Porous PDLLA Fibrous Membranes

An amount of PDLLA was successively dissolved in the solvent of DCM to prepare a 10% (w/v) polymer solution. The polymer solution was placed into a 5 mL syringe with a needle of 0.5 mm inner diameter and was pumped using a syringe pump at a rate of 25 $\mu\text{L}/\text{min}$. The electrospinning voltage was 15 kV and the tip-to-collector distance was 18 cm. The ambient humidity was controlled at 50%, 65% and 80%, respectively. The environment temperature was 15 °C, 20 °C and 25 °C, respectively. The porous PDLLA fibrous membranes were then placed into a vacuum drying oven for 2 days at 40 °C to remove residual solvent.

2.2.2. Preparation of nHA Particles

To obtain suspensions of nHA particles, a solution of H_3PO_4 was dripped into a basic suspension of $\text{Ca}(\text{OH})_2$ at a rate of 1 mL/min and stirred continuously for 12 h. The Ca:P ratio used was 1.67 and

the reaction temperature was controlled at 55 °C. The reaction mixture was then aged for 24 h at room temperature. Finally, the wet nHA was separated by high speed centrifuge at 5000 rpm and washed several times with distilled water and absolute ethyl alcohol [11,12,24].

2.2.3. Preparation of PDLLA/nHA Composite Fibrous Membranes

The nHA dispersions with different contents (10 mg/mL, 5 mg/mL, 2.5 mg/mL, 1 mg/mL and 0.5 mg/mL) were produced by ultrasonic dispersion nHA particles in a 50% (*v/v*) water/ethyl alcohol solution for about 30 min, and the porous PDLLA fibrous membrane was cut manually into 40 × 40 mm pieces. Next, the porous PDLLA fibrous membranes were bathed in nHA dispersions and oscillated for 30 min at room temperature. The coated PDLLA membranes were dipped into the absolute ethyl alcohol for 30 min for shrinking and washed five times with absolute ethyl alcohol. Finally, the PDLLA/nHA composite fibrous membranes were dried at 37 °C in a vacuum drying oven for one day.

2.3. Measurements and Characterization

The morphology of porous PDLLA fibrous membranes and the PDLLA/nHA composite fibrous membranes after gold-sputtering were observed under a scanning electron microscope (SEM, Shimadzu SSX-550) at an accelerating voltage of 3 kV. The phase of nHA was investigated by XRD using a diffractometer system (D/max-rB) equipped with monochromic Cu Ka. XRD pattern was recorded over a diffraction angle (2θ) ranging from 10° to 60° in 0.02° increments. Infrared spectra of the samples were recorded with a Fourier transform infrared spectrometer (FTIR, IRAffinity-1, Shimadzu, Kyoto, Japan) at a resolution of 2 cm⁻¹. Thermo-gravimetric Analysis (TGA) was recorded on a Pyris Diamond TG/DTA (Perkin Elmer, Waltham, Massachusetts, USA) under a 50 mL/min nitrogen flow ratio from 50 to 600 °C at a heating rate of 10 °C/min. The weight of samples was around 10 mg. The nHA content was calculated from the TGAs of the mixture ingredients' weight loss. Water contact angles were measured with a JC2000C2 contact angle goniometer (Shanghai Zhongchen Powereach Company, Shanghai, China) by the sessile drop method with a microsyringe at 25 °C. More than 10 contact angles were averaged to obtain a reliable value for each sample. Mechanical properties were performed in a Shimadzu Universal Testing Machine (AG-IS with a 10 N load cell) in tensile mode, at a strain rate of 0.5 mm/min. From the stress-strain data, the elasticity modulus was calculated. The values presented were calculated as the mean and standard deviation of the five individual measurements performed for each sample.

2.4. In Vitro Investigation

Cell culturing of chondrocytes from New Zealand white rabbits was conducted according to references [25,26]. All animal experiments were approved by the Medical Ethics Committee of Jilin University, People's Republic of China. Fibrous scaffolds were cut into circular discs with a diameter of 5 mm, sterilized with 75% ethanol for 30 min before being washed three times with Han's solution, and subsequently placed on the base of a 96-well culture dish (TPP, Transadingen, Switzerland). Scaffolds were immersed in cell culture media overnight, in an incubator (Binder, Tuttlingen, Germany). Cell suspensions were then seeded on to the scaffolds. The cultures were maintained at 37 °C in a humidified atmosphere containing 5% CO₂. SEM and confocal laser scanning microscopy (CLSM) was used to characterize cell morphology seeded on the scaffolds. Cell fixation was prior to SEM observations. After removal of the culture medium, the samples were fixed with 4% paraformaldehyde at 4 °C for 30 min and washed twice with 37 °C phosphate balanced solution. The samples for SEM images were dehydrated in an ethanol solution of increasing concentrations (30, 50, 70, 90 and 100%, respectively) for 2 min at each concentration before dried in 100% hexamethyldisilazane for 5 min. After being completely dried in air, samples were coated with gold, and observed by SEM. For CLSM observations, samples were treated with a special care route which was reported elsewhere [27].

Afterward, all samples were rinsed in phosphate balanced solution before visualized under a confocal laser scanning microscope system (FV1000-1000, Olympus, Hamburg, Germany).

3. Results and Discussion

3.1. Porous PDLLA Fibers and nHA Particles Features

The morphology of porous PDLLA fibers could be affected by electrospun ambient humidity. At a humidity of 50%, the as-spun PDLLA fibers are smooth and featureless as shown in Figure 1A. Increasing the humidity to 65% caused a visible difference in the surface morphology of the fibers. Figure 1B shows that the fibers surface contains a relatively small number of uniform, oval pores randomly distributed on the surface of the fibers. The most dramatic difference was observed when the fibers were electrospun under the highest achievable humidity of 80%. Figure 1C shows that at this increased humidity the pores are abundant on the surface of fibers, leaving little space between adjacent pores. The average pore size is in the order of 100 nm in width and 400 nm in length, with the long axis being oriented along the fiber's axis. The possible mechanism for pore formation is phase separation. A nonsolvent vapor causes phase separation of the polymer solution. In this case, electrospun ambient water is the nonsolvent, which induces the phase separation of the homogeneous mixture of PDLLA and DCM [28]. Therefore, the number of pores and their diameter on the surface of PDLLA fibers increases with increasing ambient humidity. The elongation of the pores along the fiber's axis was the result of a uniaxial extension of the jet in the electric field [29]. Furthermore, Figure 1 shows that humidity also influences the diameter of the as-spun PDLLA fibers in this experiment. As the electrospun ambient humidity increases, the mean diameter of fibers increases from 0.8 to 1.2 μm .

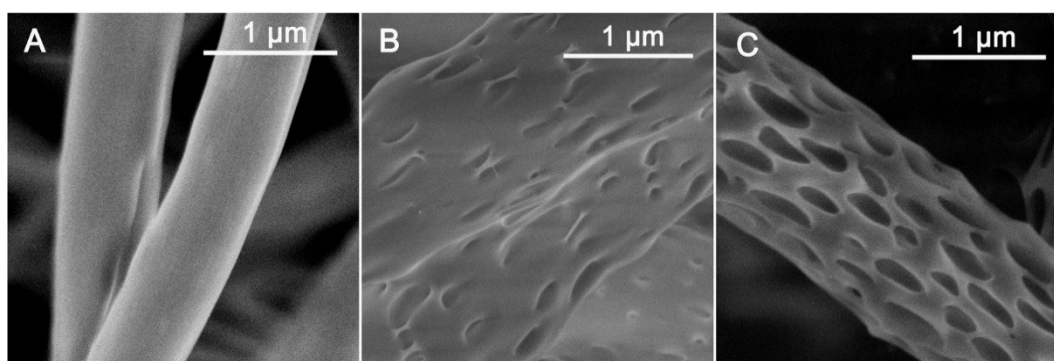


Figure 1. SEM of PDLLA fibers electrospun with different humidity at 25 °C. (A) 50%; (B) 65%; (C) 80%.

Further investigations into the environment temperature effects on the surface features of electrospun PDLLA fibers allowed for a more comprehensive look at the role of humidity in the electrospinning process. The PDLLA fibers electrospun at 15 °C showed smooth surface morphology (Figure 2A). Increasing the environment temperature to 20 °C, the as-spun fiber's surface contains a relatively small number of uniform, oval pores randomly distributed on the surface of the PDLLA fibers (Figure 2B). Figure 2C shows that the pores obtained at 25 °C were uniform in shape and were slightly larger than those obtained at other temperatures. Thermodynamic instability is another driving force behind phase separation. Increasing the ambient temperature could accelerate the volatilization of DCM. During the electrospinning process, a more rapid evaporation of the solvent as the jet was being projected from the needle causes lowering of the temperature on the fibers [30]. Pore formation begins when the temperature reaches the bimodal temperature and continues to grow until the crystallization temperature is reached [31]. These situations were encountered, thus making phase separation a likely contributing mechanism of pore formation [28]. Obviously, the humidity and environment temperature have a large effect on the morphology of the fibers' surface. In follow-up experiments, the

best electrospinning environmental conditions (25 °C and 80% humidity) to fabricate porous PDLLA fibers with good morphology was used. The mean diameter of porous fiber is around 1.2 μm .

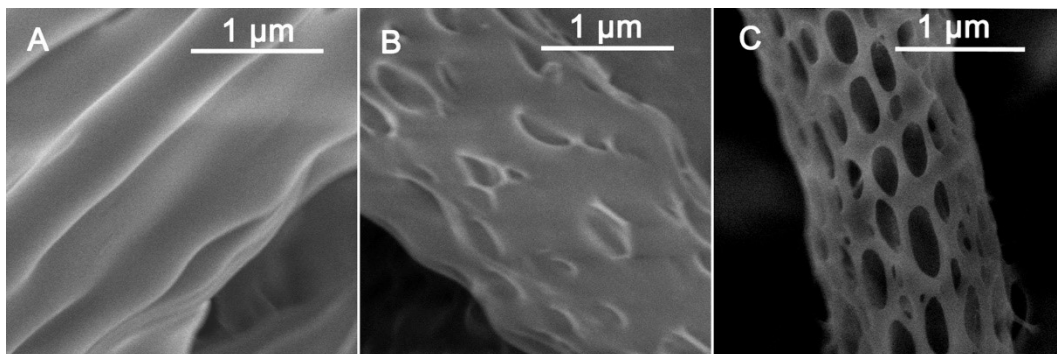


Figure 2. SEM of PDLLA fibers electrospun with different temperature under 80% humidity, (A) 15 °C; (B) 20 °C; (C) 25 °C.

The XRD patterns of nHA particles are shown in Figure 3. Based on Figure 3a, the characteristic diffraction peak at 2θ of 25.9°, 31.8°, 32.2° and 32.9°, which are assigned to [0 0 2], [2 1 1], [1 1 2] and [3 0 0] lattice planes of nHA, indicates the XRD standard card of HA JCPDS:09-0432 (Figure 3b). It was confirmed that nHA particles were successfully prepared.

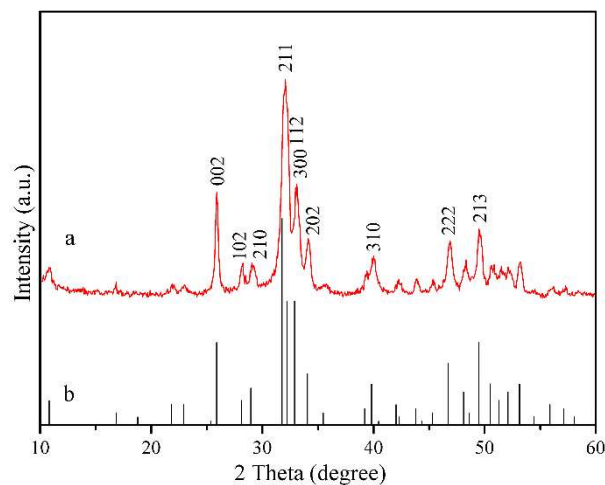


Figure 3. XRD of nHA particles, (a) self-made sample; (b) standard card.

3.2. Morphology of PDLLA/nHA Composite Fibrous Membrane

The morphology, distribution and partially enlarged detail of nHA particles on the nHA/PDLLA composite fibrous membrane were evaluated by SEM, as shown in Figure 4 (nHA particles content 10.6 wt %). As can be seen from the image, the diameter of composite fiber is around 1.0 μm , and the nHA particles are of a needle-like shape with dimensions of around 100 nm \times 20 nm. It can also be seen that the surface of the composite fiber was covered with a significant amount of nHA particles. The dispersion of nHA within the composites was uniform, and only tiny agglomeration can be seen hanging on the surface of composite fiber from the SEM image.

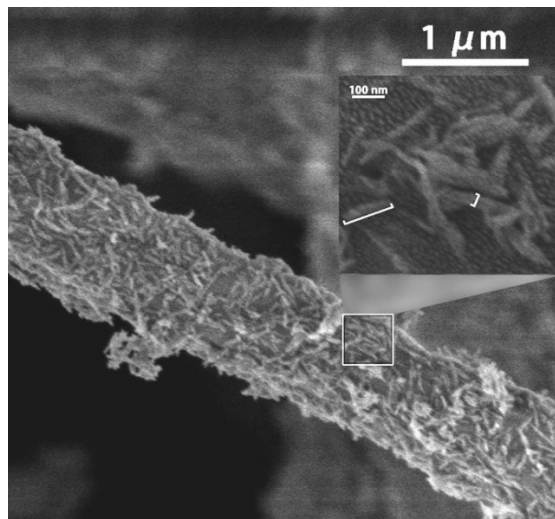


Figure 4. SEM of PDLLA/nHA composite fibers and partially enlarged detail.

3.3. FTIR of PDLLA/nHA Composite Fibrous Membrane

FTIR analysis could provide some insights into the formation of PDLLA/nHA composite fibrous membrane; the results are presented in Figure 5. Compared with the spectrum of porous PDLLA membrane (Figure 5a) and the porous PDLLA membrane shrunken in absolute ethyl alcohol without immersing into nHA dispersions (Figure 5b), the presence of the same absorption bands, indicated that the shrinking process of the PDLLA porous membrane is a physical process. The characteristic adsorption peaks of PDLLA at 1750 cm^{-1} , which were attributed to a strong C=O peak in carboxylic acid and carbonyl moieties; the band at 1089 and 1180 cm^{-1} was assigned to C-O stretching vibration bands. The bands at 1451 and 1381 cm^{-1} corresponded to the C-H scissor bending vibrations [32,33]. Compared with the spectrum of PDLLA/nHA composite fibrous membranes, seen from Figure 5b,c, the specific adsorption peaks of PO_4^{3-} at 1033 , 603 and 564 cm^{-1} were found [32]. And the typical adsorption peaks of PDLLA were not changed, demonstrating that the adsorption of the nHA particles and the shrinking of the mats occurred via all physical processes. The PDLLA/nHA composite fibrous membrane was formed by physical adsorption.

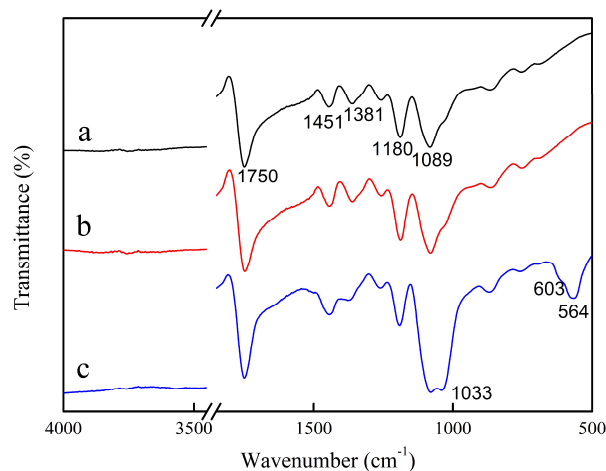


Figure 5. FTIR of (a) porous PDLLA membrane; (b) porous PDLLA membrane shrank in absolute ethyl alcohol; (c) PDLLA/nHA composite fibrous membrane.

3.4. Features of nHA/PDLLA Composite Fibrous Membranes with Different nHA Content

3.4.1. Morphologies of PDLLA/nHA Composite Fibrous Membranes

Figure 6 illustrates SEM micrographs showing the morphologies of different PDLLA/nHA composite fibrous mats by immersing and shrinking the porous PDLLA and non-porous PDLLA membrane in the nHA particles dispersions with different nHA content (10 mg/mL, 5 mg/mL, 2.5 mg/mL, 1 mg/mL and 0.5 mg/mL). The mean diameters of composite fibers are around 1.2 μm , except sample A (more than 2 μm in diameter). The literature shows that hydroxyapatite does not show any degradation up to 1000 $^{\circ}\text{C}$ [34]. Pyrolysis of PLA was almost completed at 450 $^{\circ}\text{C}$ under nitrogen condition [35,36]. Therefore, the nHA content of the different PDLLA/nHA composite fibrous membrane samples was studied with a TGA in an inert atmosphere, the results of which are shown in Table 1. Figure 6A shows that the fibers' surface of sample A was completely covered by nHA particles, with significant nHA agglomeration between fibers. The TGA indicates that the nHA content of sample A is 11.2 wt % (Table 1, sample A). The fibers' surface of sample B, which embedded 10.6 wt % nHA in the composite fibrous mats, was also completely covered with nHA particles. Tiny nHA agglomeration in the mats was still observed between fibers. From Figure 6C–E, parts of the fibers' surface were not completely covered by nHA, because of further reduction in concentration of nHA particles' dispersion. There was not enough nHA particles for adsorbing on the surface of porous PDLLA fibers in a certain amount of time.

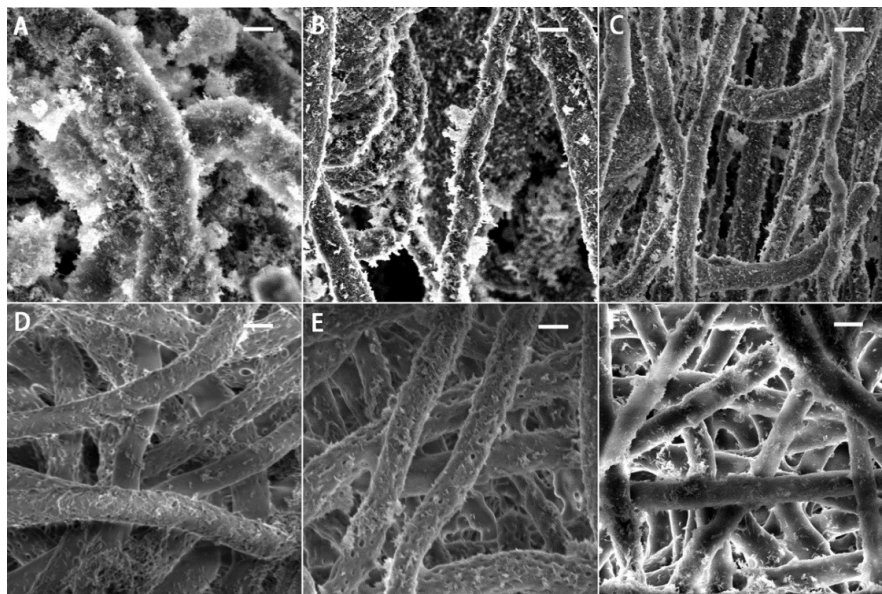


Figure 6. SEM of PDLLA/nHA composite fibrous membranes with different nHA content. Scale bars represent 1 μm .

Table 1. nHA content of PDLLA/nHA composite fibrous membranes.

Sample	A	B	C	D	E	F
nHA (wt %)	11.2	10.6	8.8	5.5	4.1	1.9

The nHA content of sample C was significantly increased compared with the control group (sample F in Figure 6 and Table 1), which was prepared by immersing non-porous PDLLA fibers in an nHA dispersion (2.5 mg/mL). And the sample C was produced by the same nHA dispersion (2.5 mg/mL). SEM indicates that there were few nHA particles adsorbed on the fibers' surface of non-porous PDLLA fibrous mats (Control group), and the nHA content of the composite mats was

only 1.9 wt %. (The nHA content of sample C is 8.8 wt %). The pore on the PDLLA fiber surface is the other key factor that influence the nHA adsorption. It is therefore demonstrated that the nHA particles' distribution and the content of PDLLA/nHA composite fibrous mats were both influenced by the pores on the PDLLA fibers and the concentration of nHA dispersion [37]. Nano-HA particles coated on the composite fibers surface will directly affect the surface wettability and mechanical property of PDLLA/nHA composite fibrous scaffold.

3.4.2. Water Contact Angles of PDLLA/nHA Composite Fibrous Membranes

Surface wettability can affect the practical application of scaffold materials in tissue engineering. The strong hydrophobicity of the scaffolds would not be conducive to cells adhesion and crawl quickly [38,39]. From Figure 6-Control, non-porous PDLLA fibrous membrane obtained by electrospinning possesses a water contact angle (WCA) of 118° . This means that the mat showed high surface hydrophobicity [40]. The introduction of hydrophilic nHA particles could significantly improve the hydrophilicity of the fibrous membrane. The relationship between the nHA particles content and the WCA of the PDLLA/nHA composite fibrous membranes is shown in Figure 7A–E. The water droplet could drop into the composite fibrous membranes' content of nHA particles at 10.6 wt % and 11.2 wt %, in a time span of two seconds, and the resulting WCA reached equilibrium was at 0° . They showed the excellent hydrophilicity because lots of nHA particles adsorbed on the surface of composite fibers. When the nHA content was reduced to 8.8 wt %, the WCA increased to 67° (Figure 7C). The WCA further increased to 89° and 104° for the composite fibrous membranes with 5.5 wt % and 4.1 wt % nHA, respectively (Figure 7D,E). It follows that the composite fibrous membranes with 10.6 wt % and 11.2 wt % nHA provided good hydrophilicity, which would help cells adsorbing quickly. The mechanical properties of PDLLA/nHA composite fibrous membranes were further investigated.

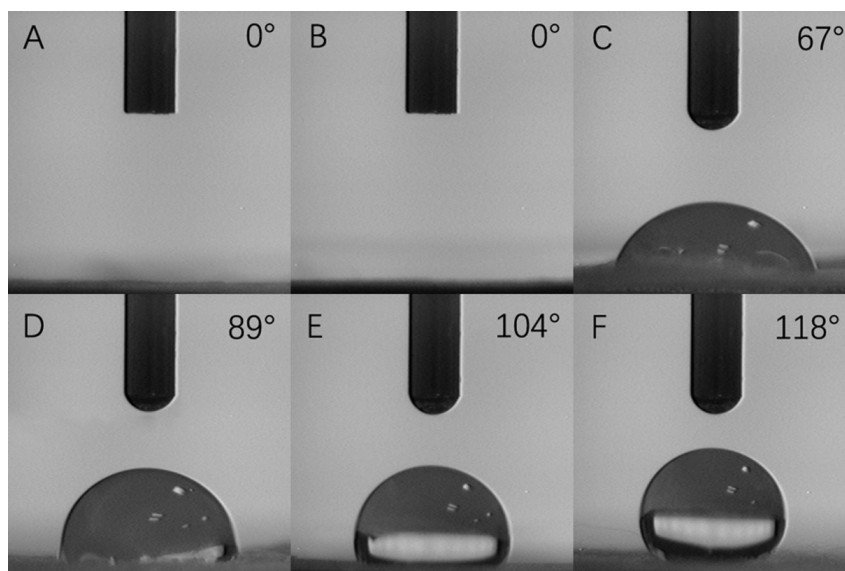


Figure 7. WCA of PDLLA/nHA membranes with different content of nHA, (A) 11.2%; (B) 10.6%; (C) 8.8%; (D) 5.5%; (E) 4.1% and (F) Control group.

3.4.3. Mechanical Property of PDLLA/nHA Composite Fibrous Membranes

Figure 8 shows the stress-strain curves of the PDLLA/nHA composite fibrous membranes and non-porous PDLLA fibrous membrane (Control group). The tensile strength and Young's modulus of these specimens are listed in Table 2. The non-porous PDLLA fibrous membranes exhibits a high modulus of 84.81 MPa and a tensile strength of 6.13 MPa (in the control group of Table 2) [41].

By adding 4.1 wt % nHA to the PDLLA composite membranes, significant reduction in the modulus and tensile strength were observed, a 60.7% and 9.3% decrease, respectively. Further modulus and tensile strength impairment to 66.8% and 44.5% can be achieved by incorporating 8.8% nHA into the PDLLA composite fibrous membranes. At 11.2% nHA loading, the modulus and tensile strength of the composite membranes declined by 76.2% and 47.1%, respectively.

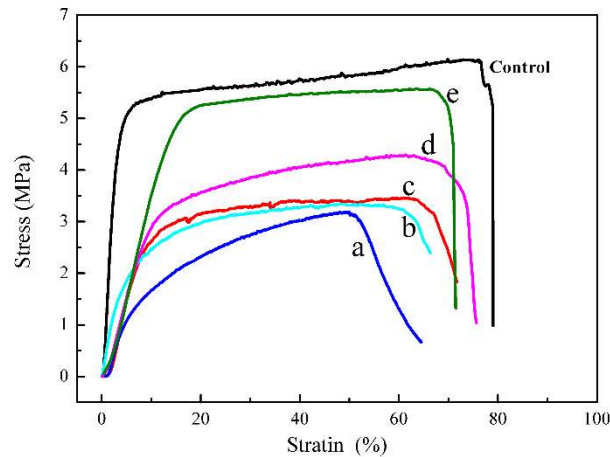


Figure 8. Tensile test of PDLLA/nHA composite fibrous membranes.

Table 2. Tensile strength and modulus of PDLLA/nHA composite fibrous membranes.

Sample	nHA (wt %)	Young's Modulus (MPa)	Tensile Strength (MPa)
a	11.2	20.19	3.24
b	10.6	26.30	3.28
c	8.8	28.19	3.40
d	5.5	31.79	4.21
e	4.1	33.34	5.56
Control	0	84.81	6.13

The presence of nHA particles in composite fibrous membranes reduces the modulus and tensile strength, because the nHA particles rendered the electrospun fiber matrix stiffer and less plastic in its deformation, in a manner which was typical of hard inorganic phases [41,42]. In general, scaffolds for tissue engineering applications should possess well surface wettability and high mechanical strength, so that they can provide load support for cell adhesion and proliferation quickly. From Table 2, the hybridization of a 10.6 wt % nHA-PDLLA composite fibrous membrane exhibits a more balanced strength and surface wettability of the composite mats, rendering a promising scaffold material for tissue engineering applications [43].

3.5. Morphology of Cell Proliferation on PDLLA/nHA Composite Fibrous Membrane

Figure 9 shows the SEM images of cells growing on non-porous PDLLA fibrous membrane (Control group) and PDLLA/nHA composite fibrous membrane (nHA particles content 10.6 wt %). Chondrocytes from rabbit could adhere to, spread and penetrate both the PDLLA and PDLLA/nHA composite fibrous scaffolds in 24 h, suggesting that the scaffolds were non-toxic. However, an undifferentiated mass formed by chondrocytes randomly dividing on the PDLLA/nHA composite fibrous scaffold was significantly larger and flatter than that on the non-porous PDLLA fiber membranes after three days. Cultured seven days later, the area of tissue pieces was further enlarged, and the surface of PDLLA/nHA composite fibrous scaffold was almost completely covered by chondrocytes. Correspondingly, morphology of the tissue block on the non-porous PDLLA fiber mats showed no remarkable change from day three to day seven. This indicates that the nHA particles

on the fibers surface of PDLLA/nHA composite scaffold could promote the adhesion and proliferation of chondrocytes from rabbits [44].

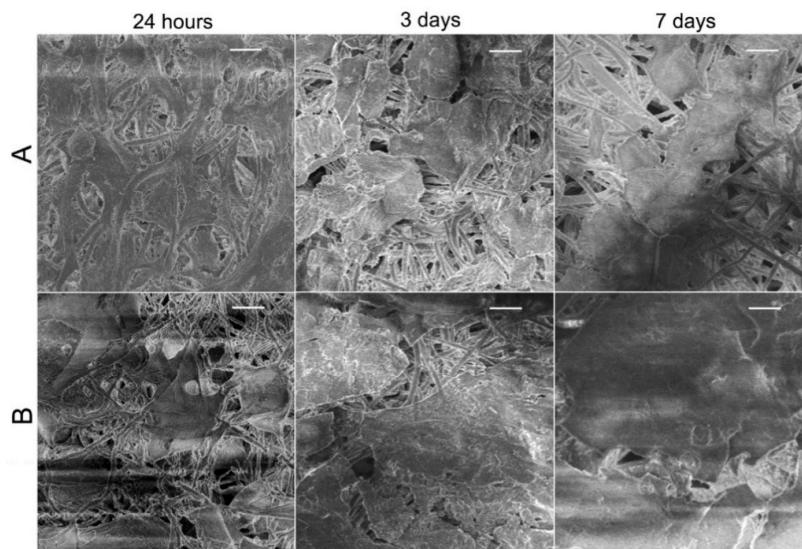


Figure 9. SEM of chondrocyte proliferation on (A) non-porous PDLLA fibrous membrane; (B) PDLLA/nHA composite fibrous membrane. Scale bars represent 10 μm .

Immunofluorescence combined with CLSM observation further showed that both PDLLA and PDLLA/nHA composite fibrous scaffolds could support chondrocytes adhesion and proliferation (Figure 10). Viability of chondrocytes cultured on two kinds of fibrous scaffolds for 24 h revealed the same cell density. After three days, chondrocytes on PDLLA/nHA composite fibrous scaffold displayed higher proliferative capability (Figure 10B-3 days), which indicated that composite scaffold could enhance proliferation of chondrocytes. On the contrary, chondrocytes proliferation on PDLLA fibrous scaffold showed a non-uniform cell distribution (Figure 10A-3 days). Cultured 7 days later, the composite fibrous scaffold was significantly improved the proliferation of the chondrocytes, which show PDLLA/nHA composite fibrous scaffold could more benefit for chondrocytes proliferation.

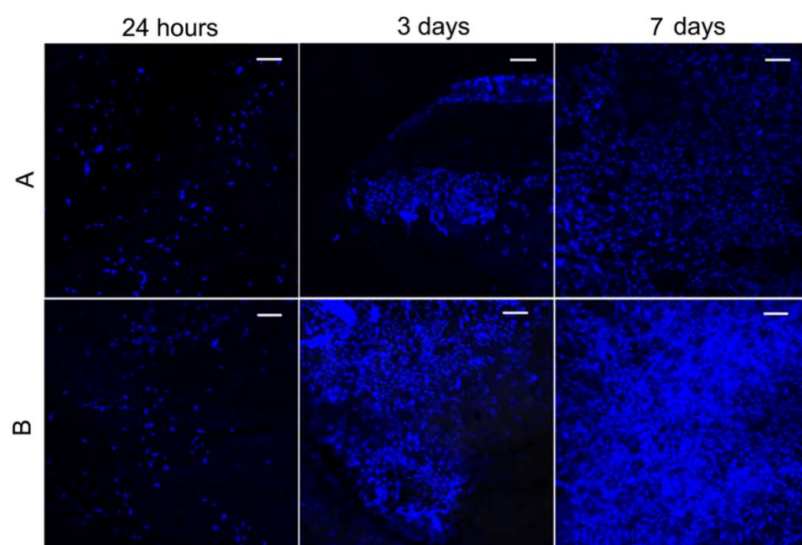


Figure 10. CLSM of chondrocytes proliferation on (A) non-porous PDLLA fibrous membrane; (B) PDLLA/nHA composite fibrous membrane. Scale bars represent 100 μm .

4. Conclusions

Composite fibrous membranes were prepared from PDLLA and nHA at different wt % HA content through electrospinning and dipping in turn. Based on the pore morphology of porous PDLLA fiber surface studied, the best electrospinning environment in which to fabricate fibers with good morphology was confirmed (temperature 25 °C and humidity 80%). FTIR showed that the nHA particles were embedded on the PDLLA surface by physical adsorption.

A batch of PDLLA/nHA composite fibrous membranes was prepared by dipping porous PDLLA fiber mats into nHA particles dispersionns with different nHA content. Morphology analysis indicates that, as more nHA particles are adsorbed onto the fiber surface, the content of nHA dispersion increases. There was significant nHA agglomeration between fibers, when the nHA content of fibers increased to 11.2 wt %. When the mass fraction of hydrophilic nHA particles was over 10.6%, the surface wettability of composite fibrous membranes was significantly improved. Water droplets could penetrate the fiber membrane rapidly in two seconds. Although the presence of nHA particles in the composite fibrous membranes reduces the modulus and tensile strength, the 10.6 wt % PDLLA/nHA composite fibrous membrane exhibits a more balanced surface wettability and tensile strength of the composite mats. In vitro study showed that the composite scaffold is non-toxic. The adherence and proliferation of chondrocytes on the 10.6 wt % PDLLA/nHA fibrous membrane was significantly improved, compared with PDLLA fibrous mat. This composite membrane has potential application value as scaffold material in tissue engineering. Further research would, however, focus on the in vitro degradation progress in order to provide the references for in vivo histocompatibility.

Author Contributions: Linhui Qiang wrote the manuscript; Cong Zhang conceived, designed and performed the experiments; Linhui Qiang, Feng Qu and Xiaonan Wu contributed to the analysis of results; Cong Zhang analysed the cell experimental; Hongyan Wang contributed to the analysis of results, provided feedback to the content and participated in writing the manuscript.

Acknowledgments: This work was supported by the National Natural Science Foundation of China (No. 21104023).

Conflicts of Interest: The authors declare no conflict of interest.

References

1. Khademhosseini, A.; Langer, R. A decade of progress in tissue engineering. *Nat. Protoc.* **2016**, *11*, 1775. [[CrossRef](#)] [[PubMed](#)]
2. Zhu, W.; Ma, X.; Gou, M.; Mei, D.; Zhang, K.; Chen, S. 3D printing of functional biomaterials for tissue engineering. *Curr. Opin. Biotechnol.* **2016**, *40*, 103–112. [[CrossRef](#)] [[PubMed](#)]
3. Liu, M.; Zeng, X.; Ma, C.; Yi, H.; Ali, Z.; Mou, X.; Li, S.; Deng, Y.; He, N. Injectable hydrogels for cartilage and bone tissue engineering. *Bone Res.* **2017**, *5*, 17014. [[CrossRef](#)] [[PubMed](#)]
4. Klotz, B.J.; Gawlitta, D.; Rosenberg, A.J.; Malda, J.; Melchels, F.P. Gelatin-methacryloyl hydrogels: Towards biofabrication-based tissue repair. *Trends Biotechnol.* **2016**, *34*, 394–407. [[CrossRef](#)] [[PubMed](#)]
5. Liu, W.; Thomopoulos, S.; Xia, Y. Electrospun nanofibers for regenerative medicine. *Adv. Healthc. Mater.* **2012**, *1*, 10–25. [[CrossRef](#)] [[PubMed](#)]
6. Xu, T.O.; Kim, H.S.; Stahl, T.; Nukavarapu, S.P. Self-neutralizing PLGA/magnesium composites as novel biomaterials for tissue engineering. *Biomed. Mater.* **2018**, *13*, 035013. [[CrossRef](#)] [[PubMed](#)]
7. Wu, D.; Samanta, A.; Srivastava, R.K.; Hakkarainen, M. Nano-Graphene Oxide Functionalized Bioactive Poly(lactic acid) and Poly(ϵ -caprolactone) Nanofibrous Scaffolds. *Materials* **2018**, *11*, 566. [[CrossRef](#)] [[PubMed](#)]
8. Ishii, D.; Ying, T.H.; Yamaoka, T.; Iwata, T. Characterization and Biocompatibility of Biopolyester Nanofibers. *Materials* **2009**, *2*, 1520–1546. [[CrossRef](#)]
9. Liu, Y.; Wang, S.; Zhang, R. Composite poly (lactic acid)/chitosan nanofibrous scaffolds for cardiac tissue engineering. *Int. J. Biol. Macromol.* **2017**, *103*, 1130–1137. [[CrossRef](#)] [[PubMed](#)]
10. Turon, P.; del Valle, L.J.; Alemán, C.; Puiggalí, J. Biodegradable and Biocompatible Systems Based on Hydroxyapatite Nanoparticles. *Appl. Sci.* **2017**, *7*, 60. [[CrossRef](#)]

11. Dou, T.; Jing, N.; Zhou, B.; Zhang, P. In vitro mineralization kinetics of poly (L-lactic acid)/hydroxyapatite nanocomposite material by attenuated total reflection Fourier transform infrared mapping coupled with principal component analysis. *J. Mater. Sci.* **2018**, *53*, 8009–8019. [[CrossRef](#)]
12. Ruphuy, G.; Souto-Lopes, M.; Paiva, D.; Costa, P.; Rodrigues, A.E.; Monteiro, F.J.; Salgado, C.L.; Fernandes, M.H.; Lopes, J.C.; Dias, M.M.; et al. Supercritical CO₂ assisted process for the production of high-purity and sterile nano-hydroxyapatite/chitosan hybrid scaffolds. *J. Biomed. Mater. Res. B* **2018**, *106*, 965–975. [[CrossRef](#)] [[PubMed](#)]
13. Sariibrahimoglu, K.; Yang, W.; Leeuwenburgh, S.C.; Yang, F.; Wolke, J.G.; Zuo, Y.; Li, Y.; Jansen, J.A. Development of porous polyurethane/strontium-substituted hydroxyapatite composites for bone regeneration. *J. Biomed. Mater. Res. A* **2015**, *103*, 1930–1939. [[CrossRef](#)] [[PubMed](#)]
14. De Aza, P.N.; Rodríguez, M.A.; Gehrke, S.A.; Maté-Sánchez de Val, J.E.; Calvo-Guirado, J.L. A Si- α TCP Scaffold for Biomedical Applications: An Experimental Study Using the Rabbit Tibia Model. *Appl. Sci.* **2017**, *7*, 706. [[CrossRef](#)]
15. Hinderer, S.; Layland, S.L.; Schenke-Layland, K. ECM and ECM-like materials—biomaterials for applications in regenerative medicine and cancer therapy. *Adv. Drug Deliv. Rev.* **2016**, *97*, 260–269. [[CrossRef](#)] [[PubMed](#)]
16. Shalumon, K.T.; Anjana, J.; Mony, U.; Jayakumar, R.; Chen, J.P. Process study, development and degradation behavior of different size scale electrospun poly (caprolactone) and poly (lactic acid) fibers. *J. Polym. Res.* **2018**, *25*, 82. [[CrossRef](#)]
17. Xu, T.; Yang, H.; Yang, D.; Yu, Z.Z. Polylactic Acid Nanofiber Scaffold Decorated with Chitosan Islandlike Topography for Bone Tissue Engineering. *ACS Appl. Mater. Interfaces* **2017**, *9*, 21094–21104. [[CrossRef](#)] [[PubMed](#)]
18. Santos, D.; Correia, C.O.; Silva, D.M.; Gomes, P.S.; Fernandes, M.H.; Santos, J.D.; Sencadas, V. Incorporation of glass-reinforced hydroxyapatite microparticles into poly (lactic acid) electrospun fibre mats for biomedical applications. *Mater. Sci. Eng. C-Mater.* **2017**, *75*, 1184–1190. [[CrossRef](#)] [[PubMed](#)]
19. Su, C.J.; Tu, M.G.; Wei, L.J.; Hsu, T.T.; Kao, C.T.; Chen, T.H.; Huang, T.H. Calcium silicate/chitosan-coated electrospun poly (lactic acid) fibers for bone tissue engineering. *Materials* **2017**, *10*, 501. [[CrossRef](#)] [[PubMed](#)]
20. Grémare, A.; Guduric, V.; Bareille, R.; Heroguez, V.; Latour, S.; L'heureux, N.; Fricain, J.-C.; Catros, S.; Le Nihouannen, D. Characterization of printed PLA scaffolds for bone tissue engineering. *J. Biomed. Mater. Res. A* **2018**, *106*, 887–894.
21. Narayanan, G.; Vernekar, V.N.; Kuyinu, E.L.; Laurencin, C.T. Poly (lactic acid)-based biomaterials for orthopaedic regenerative engineering. *Adv. Drug Deliv. Rev.* **2016**, *107*, 247–276. [[CrossRef](#)] [[PubMed](#)]
22. Zeng, Y.; Yan, Y.; Yan, H.; Liu, C.; Li, P.; Dong, P.; Zhao, Y.; Chen, J. 3D printing of hydroxyapatite scaffolds with good mechanical and biocompatible properties by digital light processing. *J. Mater. Sci.* **2018**, *53*, 6291–6301. [[CrossRef](#)]
23. Della Bella, E.; Parrilli, A.; Bigi, A.; Panzavolta, S.; Amadori, S.; Giavaresi, G.; Martini, L.; Borsari, V.; Fini, M. Osteoinductivity of nanostructured hydroxyapatite-functionalized gelatin modulated by human and endogenous mesenchymal stromal cells. *J. Biomed. Mater. Res. A* **2018**, *106*, 914–923. [[CrossRef](#)] [[PubMed](#)]
24. Gentile, P.; Wilcock, C.J.; Miller, C.A.; Moorehead, R.; Hatton, P.V. Process optimisation to control the physico-chemical characteristics of biomimetic nanoscale hydroxyapatites prepared using wet chemical precipitation. *Materials* **2015**, *8*, 2297–2310. [[CrossRef](#)]
25. Alaminos, M.; Sánchez-Quevedo, M.D.C.; Muñoz-Ávila, J.I.; Serrano, D.; Medialdea, S.; Carreras, I.; Campos, A. Construction of a complete rabbit cornea substitute using a fibrin-agarose scaffold. *Investig. Ophthalmol. Vis. Sci.* **2006**, *47*, 3311–3317. [[CrossRef](#)] [[PubMed](#)]
26. Orwin, E.J.; Hubel, A. In vitro culture characteristics of corneal epithelial, endothelial, and keratocyte cells in a native collagen matrix. *Tissue Eng.* **2000**, *6*, 307–319. [[CrossRef](#)] [[PubMed](#)]
27. Yan, J.; Qiang, L.; Gao, Y.; Cui, X.; Zhou, H.; Zhong, S.; Wang, Q.; Wang, H. Effect of fiber alignment in electrospun scaffolds on keratocytes and corneal epithelial cells behavior. *J. Biomed. Mater. Res. A* **2012**, *100*, 527–535. [[CrossRef](#)] [[PubMed](#)]
28. Casper, C.L.; Stephens, J.S.; Tassi, N.G.; Chase, D.B.; Rabolt, J.F. Controlling surface morphology of electrospun polystyrene fibers: Effect of humidity and molecular weight in the electrospinning process. *Macromolecules* **2004**, *37*, 573–578. [[CrossRef](#)]
29. Bognitzki, M.; Czado, W.; Frese, T.; Schaper, A.; Hellwig, M.; Steinhart, M.; Greiner, A.; Wendorff, J.H. Nanostructured fibers via electrospinning. *Adv. Mater.* **2001**, *13*, 70–72. [[CrossRef](#)]

30. Wijmans, J.G.; Smolders, C.A. Preparation of asymmetric membranes by the phase inversion process. *Synth. Membr. Sci. Eng. Appl.* **1996**, *39*, 39–56. [[CrossRef](#)]
31. Matsuyama, H.; Maki, T.; Teramoto, M.; Asano, K. Effect of polypropylene molecular weight on porous membrane formation by thermally induced phase separation. *J. Membr. Sci.* **2002**, *204*, 323–328. [[CrossRef](#)]
32. Mao, D.; Li, Q.; Bai, N.; Dong, H.; Li, D. Porous stable poly (lactic acid)/ethyl cellulose/hydroxyapatite composite scaffolds prepared by a combined method for bone regeneration. *Carbohydr. Polym.* **2018**, *180*, 104–111. [[CrossRef](#)] [[PubMed](#)]
33. Wang, B.; Li, H.; Yao, Q.; Zhang, Y.; Zhu, X.; Xia, T.; Wang, J.; Li, G.; Li, X.; Ni, S. Local in vitro delivery of rapamycin from electrospun PEO/PDLLA nanofibers for glioblastoma treatment. *Biomed. Pharmacother.* **2016**, *83*, 1345–1352. [[CrossRef](#)] [[PubMed](#)]
34. Nazeer, M.A.; Yilgör, E.; Yilgör, I. Intercalated chitosan/hydroxyapatite nanocomposites: Promising materials for bone tissue engineering applications. *Carbohydr. Polym.* **2017**, *175*, 38–46. [[CrossRef](#)] [[PubMed](#)]
35. Petisco-Ferrero, S.; Pérez Álvarez, L.; Ruiz-Rubio, L.; Vilas Vilela, J.L.; Sarasua, J.R. Plasma poly (acrylic acid) compatibilized hydroxyapatite-poly(lactide) biocomposites for their use as body-absorbable osteosynthesis devices. *Compos. Sci. Technol.* **2018**, *161*, 66–73. [[CrossRef](#)]
36. Wan, Y.; Wu, C.; Xiong, G.; Zuo, G.; Jin, J.; Ren, K.; Zhu, Y.; Wang, Z.; Luo, H. Mechanical properties and cytotoxicity of nanoplate-like hydroxyapatite/poly(lactide) nanocomposites prepared by intercalation technique. *J. Mech. Behav. Biomed.* **2015**, *47*, 29–37. [[CrossRef](#)] [[PubMed](#)]
37. Dai, X.; Li, X.; Wang, X. Morphology controlled porous poly (lactic acid)/zeolitic imidazolate framework-8 fibrous membranes with superior PM_{2.5} capture capacity. *Chem. Eng. J.* **2018**, *338*, 82–91. [[CrossRef](#)]
38. Puppi, D.; Chiellini, F.; Piras, A.M.; Chiellini, E. Polymeric materials for bone and cartilage repair. *Prog. Polym. Sci.* **2010**, *35*, 403–440. [[CrossRef](#)]
39. Zhang, M.; Ye, L.; Gao, Y.; Lv, X.; Chang, J. Effects of hydrolysis on dodecyl alcohol modified β -CaSiO₃ particles and PDLLA/modified β -CaSiO₃ composite films. *Compos. Sci. Technol.* **2009**, *69*, 2547–2553. [[CrossRef](#)]
40. Cui, W.; Li, X.; Zhou, S.; Weng, J. Degradation patterns and surface wettability of electrospun fibrous mats. *Polym. Degrad. Stab.* **2008**, *93*, 731–738. [[CrossRef](#)]
41. Cui, W.; Li, X.; Xie, C.; Chen, J.; Zou, J.; Zhou, S.; Weng, J. Controllable growth of hydroxyapatite on electrospun poly (dl-lactide) fibers grafted with chitosan as potential tissue engineering scaffolds. *Polymer* **2010**, *51*, 2320–2328. [[CrossRef](#)]
42. Zou, B.; Liu, Y.; Luo, X.; Chen, F.; Guo, X.; Li, X. Electrospun fibrous scaffolds with continuous gradations in mineral contents and biological cues for manipulating cellular behaviors. *Acta Biomater.* **2012**, *8*, 1576–1585. [[CrossRef](#)] [[PubMed](#)]
43. Jeong, S.I.; Ko, E.K.; Yum, J.; Jung, C.H.; Lee, Y.M.; Shin, H. Nanofibrous poly (lactic acid)/hydroxyapatite composite scaffolds for guided tissue regeneration. *Macromol. Biosci.* **2008**, *8*, 328–338. [[CrossRef](#)] [[PubMed](#)]
44. Cui, W.; Li, X.; Xie, C.; Zhuang, H.; Zhou, S.; Weng, J. Hydroxyapatite nucleation and growth mechanism on electrospun fibers functionalized with different chemical groups and their combinations. *Biomaterials* **2010**, *31*, 4620–4629. [[CrossRef](#)] [[PubMed](#)]

